INORGANIC CHEMISTRY
FRONTIERS

RESEARCH ARTICLE

View Article Online
View Journal | View Issue

Cite this: *Inorg. Chem. Front.*, 2019, **6**, 2921

Enhancing C_2H_2/C_2H_4 separation by incorporating low-content sodium in covalent organic frameworks†

Yuan Tao,[a] Rajamani Krishna,[b] Li Xiao Yang,[a] Ya Ling Fan,[a] Li Wang,[a] Zhi Gao,[a] Jian Bo Xiong,[a] Li Jun Sun[a] and Feng Luo *[a]

Received 24th July 2019,
Accepted 3rd September 2019

DOI: 10.1039/c9qi00922a

rsc.li/frontiers-inorganic

The separation of C_2H_2/C_2H_4 mixtures is of industrial importance in the production of high-purity C_2H_4 and C_2H_2. The primary objective of this work is to enhance the selectivity of C_2H_2/C_2H_4 separation by developing a method for appropriate modification of porous adsorbents. Toward this end, directly doping low-content Na^+ ions into covalent organic frameworks (COFs) *via* cation exchange is proposed in this work. Relative to the pristine COF, **COF-ECUT-1**, with C_2H_2 and C_2H_4 adsorption capacities of 55.39 $cm^3\ g^{-1}$ and 28.63 $cm^3\ g^{-1}$, the Na^+-anchored phase with just 4.0 wt% sodium content, **Na@COF-ECUT-1**, enables largely enhanced adsorption ability with the corresponding values of 89.70 $cm^3\ g^{-1}$ and 49.26 $cm^3\ g^{-1}$, respectively. As a result, the adsorption selectivity of C_2H_2 over that of C_2H_4 is enhanced from 6.33 to 9.41, and the separation potential estimated by the simulated transient breakthrough is largely improved about three-fold. The density functional theory (DFT) calculation reveals that the trap of Na^+ within the COF channel affords strong affinity towards C_2H_2 or C_2H_4 through Na–π interactions and relatively stronger contact for C_2H_2 than for C_2H_4 is observed. This result is in line with the experimental results of both enhanced C_2H_2 and C_2H_4 adsorption capacity and C_2H_2/C_2H_4 separation performance. This work outlines a general and simple method to enhance the gas separation performance upon COF materials.

Introduction

Acetylene (C_2H_2) and ethylene (C_2H_4) are essential raw materials for a range of chemical products and materials. Industrially produced ethylene invariably contains a small amount of acetylene, to the level of about 1%.[1,2] This small amount of acetylene has a great influence on the production and processing of ethylene.[3,4] For example, acetylene can undergo transformation to solid metal acetylides that have undesirable properties and are also explosive in nature. On the other hand, there is demand for high purity C_2H_2 in a variety of industrial applications. However, due to that they have comparable molecular size and similar physicochemical properties, the separation of acetylene and ethylene is a challenging task.[5,6]

The conventional approaches for removing acetylene from the acetylene/ethylene mixture include selective semihydrogenation and absorption using chemical solvents such as dimethyl formamide.[4] Nevertheless, both these approaches have drawbacks such as the need for precious metal catalysts and toxic solutions; furthermore the current technologies for C_2H_2 removal involve high energy-consumption processes.[7] On the other hand, due to their comparable molecular size and similar physicochemical properties, selective adsorption with traditional porous materials such as porous carbons and zeolites is usually of low selectivity.[8,9] Recently, due to their diversity in structure and easy-to-access modification in the pore and pore wall, a new porous platform of metal–organic frameworks (MOFs), built on a metal node and an organic linker, has been viewed to be a promising candidate for mixed gas separation, especially for the gases with similar size.[10–20] Along with the appreciation in the relationship between the selective adsorption and the MOF structure and topology, several novel effective approaches for C_2H_2/C_2H_4 separation have been developed. For example, the open metal site in the pore of MOFs is suggested to give strong affinity for the C_2H_2 molecule, thus leading to selective adsorption of C_2H_2 over C_2H_4.[21] However, such a strong coordination interaction between C_2H_2 and the open metal site makes the desorption of C_2H_2 from the MOF materials a highly energy-intensive process. Moreover, the open metal site of MOFs is often extremely sensitive to the presence of water in the feed streams that

[a]*State Key Laboratory for Nuclear Resources and Environment, and School of Biology, Chemistry and Material Science, East China University of Technology, Nanchang, Jiangxi 344000, China. E-mail: ecitluofeng@163.com*
[b]*Van't Hoff Institute for Molecular Sciences, University of Amsterdam, Science Park 904, 1098 XH Amsterdam, The Netherlands*

†Electronic supplementary information (ESI) available: Experiments and additional figures. See DOI: 10.1039/c9qi00922a

cause degradation. To address this issue, in some cases constructing free-standing organic units in the pore wall of MOFs was suggested and this relatively weak hydrogen bond interaction or the van der Waals interaction indeed enables selective identification of C_2H_2 over C_2H_4.[22] In some other cases, the suitable pore size is highly important for C_2H_2/C_2H_4 separation.[23] We recently also disclosed a photosensitive MOF that enables photoswitching C_2H_2/C_2H_4 separation performance.[24]

In contrast to MOFs, their porous counterparts, covalent organic frameworks (COFs), are built on covalent bonds and strong π–π interactions, thus leading to several desirable properties such as high thermostability and chemical thermostability.[25–30] Consequently, COFs offer the potential of use in adsorptive separations. For example, COFs with free-standing thiol or amidoxime groups were confirmed to exhibit selective and high-capacity Hg or U adsorption, respectively.[31] Owing to the strong Lewis acid–base interactions, COF-10 afforded the ultrahigh uptake capacity of NH_3.[32] Recently, the possibility of enantioselective separation with COFs anchored by optically pure 1,1′-bi-2-naphthol (BINOL) units has been demonstrated.[33] PAF-110 is the first COF adsorbent developed for C_2H_2/C_2H_4 separation.[34] However, with PAF-110, the C_2H_2/C_2H_4 selectivity is only 3.9 at 298 K and 1 bar, which is significantly below the values that are desirable in practice. In this regard, constructing COFs with high acetylene selectivity, especially through a general and simple method, is highly desirable and challenging.

In this work, we found that a SO_3H-anchored COF, **COF-ECUT-1**, enables high C_2H_2/C_2H_4 selectivity up to 6.33 at 298 K and 1 bar. The selectivity can be further enhanced up to 9.41 by doping low-content Na^+ ions *via* direct cation exchange.

Results and discussion

COF-ECUT-1 was synthesized through a Schiff-base condensation reaction of 2,4,6-triformylphloroglucinol and 2,5-diaminobenzenesulfonic acid in *n*-butanol and 1,2-dichlorobenzene with aqueous acetic acid at 120 °C for 72 hours. The counterpart of **Na@COF-ECUT-1** was obtained by immersing **COF-ECUT-1** in sodium carbonate solution *via* direct cation-exchange. Their morphology was examined by scanning electron microscopy (SEM, Fig. 1), suggesting a thread configuration. Thermogravimetric analysis (TG) showed that the loading of sodium in the COF leads to enhanced thermostability (Fig. S3†). In the IR spectrum (infrared spectrum) the successful synthesis of β-ketoenamine-linked structures in **COF-ECUT-1** and **Na@COF-ECUT-1** is confirmed by the C–N band at 1272 cm^{-1}.[25–30] The bands observed at 1120 and 1076 cm^{-1}, along with a shoulder at 622 and 536 cm^{-1}, can be attributed to the O═S═O symmetric and asymmetric stretching bands; these indicate the existence of sulfonic acid. Interestingly in the IR spectra of **Na@COF-ECUT-1**, the characteristic stretching band of the OH group on sulfonate at 1480 cm^{-1} almost disappeared, mainly due to the ion exchange between H^+ and Na^+ (Fig. S4†). Moreover, the maintenance of the SO_3^- or SO_3H unit in the resulted COF materials of **COF-ECUT-1** and **Na@COF-ECUT-1** and the success of Na^+ incorporation are intuitively reflected by the elemental distribution mapping through the energy dispersive spectrometry (EDS) test (Fig. 1). The content of the Na element in the **Na@COF-ECUT-1** samples was determined to be 4.0 wt% by ICP-OES (inductively coupled plasma emission spectrometer). The COF is further confirmed by the ^{13}C CP/MAS NMR spectrum, where the assignment of carbon atoms completely matches with the β-ketoenamine-linked structure (Fig. S5†).

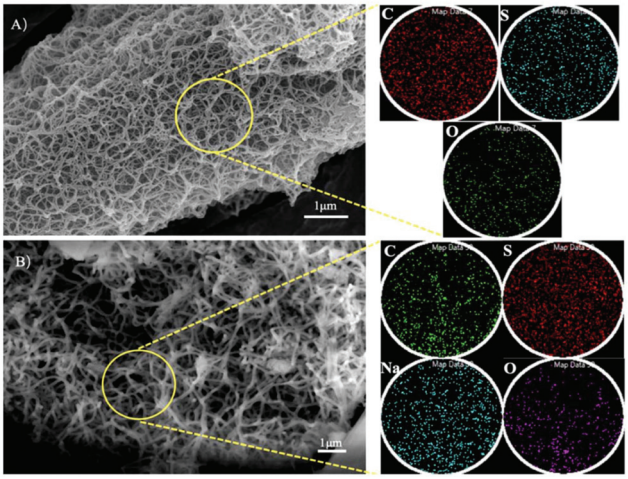

Fig. 1 SEM images of **COF-ECUT-1** (A) and **Na@COF-ECUT-1** (B). The highlights are the elemental distribution mapping.

The structure of **COF-ECUT-1** was determined by comparing the powder X-ray diffraction (PXRD) with the simulated results from the calculation performed by Materials Studio (Fig. 2 and Fig. S6†). Based on the calculation results, it is suggested that **COF-ECUT-1** crystallizes in the hexagonal $P\bar{6}$ space group with $a = b = 22.4990$ Å and $c = 6.8000$ Å and the

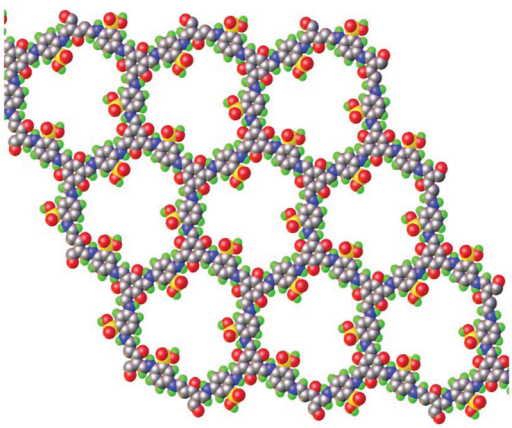

Fig. 2 View of the structure of **COF-ECUT-1**. The color code is C/grey, O/red, H/green, N/blue, and S/yellow.

packing mode shows an eclipsed structure stabilized by π–π interactions, rather than a staggered structure. However, the arrangement of SO_3H^- units among adjacent layers shows the opposite (Fig. S7†). The PXRD patterns of **Na@COF-ECUT-1** match well with those of the pristine samples of **COF-ECUT-1**, indicative of the retention of the COF structure after cation exchange (Fig. S6†).

In order to assess the porosity of **COF-ECUT-1** and **Na@COF-ECUT-1**, N_2 sorption isotherms were collected at 77 K. Both of these showed a microporous isotherm with a BET surface area of 306 $m^2\ g^{-1}$ and 149 $m^2\ g^{-1}$ and an aperture about 1.2 nm and 0.8 nm, respectively (Fig. S8†). This decrease in both the BET area and the aperture is due to the replacement of hydrogen ions from the SO_3H group with Na^+ ions.

The polar and acidic SO_3H groups with both H-donor potential and H-acceptor potential in **COF-ECUT-1** and Na^+ incorporation within the COF encouraged us to explore the storage and separation of C_2H_2 and C_2H_4. Firstly, the gas adsorption of C_2H_2 and C_2H_4 upon **COF-ECUT-1** and **Na@COF-ECUT-1** was investigated. At 298 K and 100 kPa, **COF-ECUT-1** affords a moderate acetylene adsorption capacity of 55.39 $cm^3\ g^{-1}$ (Fig. 3), which is higher than that observed for PAF-110.[34] The C_2H_4 adsorption capacity upon **COF-ECUT-1** is just 28.63 $cm^3\ g^{-1}$, far below than the C_2H_2 adsorption capacity of 55.39 $cm^3\ g^{-1}$, indicative of potential for C_2H_2/C_2H_4 separation (Fig. 4). Ideally, a porous adsorbent should have a combination of high selectivity with high uptake capacity. Most commonly, high selectivities do not go hand-in-hand with high uptake capacities. There is a need to develop a methodology to achieve high uptake capacities, without sacrificing the benefits of high selectivities. In contrast to the pristine COF samples, the counterpart of **Na@COF-ECUT-1** displays a significant enhancement by 1.6-fold in C_2H_2 adsorption capacity (89.70 $cm^3\ g^{-1}$) (Fig. 3). However, the C_2H_4 adsorption capacity increases to 49.26 $cm^3\ g^{-1}$, giving a comparable 1.7-fold enhancement (Fig. 3). Accordingly, such a large increase in the adsorption capacity from 55.39 $cm^3\ g^{-1}$ to 89.70 $cm^3\ g^{-1}$ nearly does not affect the adsorption difference (1.8-fold for **Na@COF-ECUT-1** and 1.9-fold for **COF-ECUT-1**,

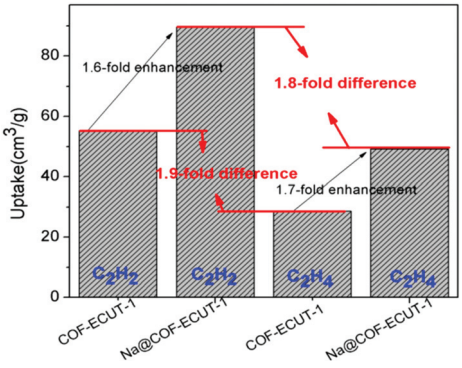

Fig. 4 Large enhancement in adsorption capacity but without obvious changes in the adsorption difference. The used data are the experimental data at 298 K and 100 kPa.

Fig. 4). Thus, the incorporation of Na^+ into the COF should be an effective method to largely enhance the C_2H_2 adsorption capacity also without sacrificing selectivity.

To quantitatively evaluate the adsorption difference observed in **COF-ECUT-1** and **Na@COF-ECUT-1**, we employed the well-known ideal adsorbed solution theory (IAST) to calculate the adsorption selectivity for a C_2H_2/C_2H_4 binary mixture (1/99, v/v).[14d] As shown in Fig. 5, **COF-ECUT-1** shows a C_2H_2/C_2H_4 selectivity of 6.33 at 100 kPa and 298 K. This value is higher than that observed for PAF-110 (3.9)[34] that represents the first reported adsorbent for C_2H_2/C_2H_4 separation in the field of COFs and the porous organic polymer of CTF-PO71 (1.8).[35] To the best of our knowledge, the obtained results appear to be a record for C_2H_2/C_2H_4 separation upon COFs. Such high C_2H_2/C_2H_4 selectivity is also comparable with some benchmark MOFs such as **NbU-1**.[36] Most importantly, the Na^+-doped phase of **Na@COF-ECUT-1** afforded large enhancement in C_2H_2/C_2H_4 selectivity up to 9.41 at 100 kPa and 298 K, which is high enough for use in industrial practice for C_2H_2/C_2H_4 separation. It is noteworthy that the Na^+ content is very low down to 4.0 wt%, which is far below the metal content within any MOFs.[20] Therefore, the Na^+-doped approach should be a powerful tool to enhance C_2H_2/C_2H_4 separation.

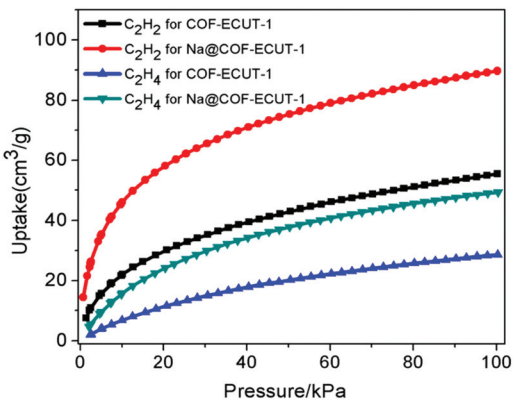

Fig. 3 The C_2H_2 and C_2H_4 uptake at 298 K for samples of **COF-ECUT-1** and **Na@COF-ECUT-1**.

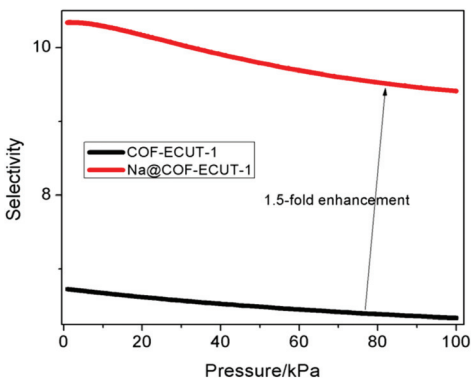

Fig. 5 The C_2H_2/C_2H_4 selectivity calculated by IAST, based on **COF-ECUT-1** and **Na@COF-ECUT-1**.

The isosteric heat of adsorption (Q_{st}) is also another important property for any porous separation material, which not only reflects the binding strength and also the difficulty of regeneration. Generally speaking, MOFs with open metal sites show strong affinity and thus high Q_{st}, but with greater difficulty in regeneration and thus higher energy cost.[14d] Thereby, a porous adsorbent with high selectivity but low Q_{st} is highly desirable. As shown in Fig. S9 and S10,† both **COF-ECUT-1** and **Na@COF-ECUT-1** show lower Q_{st} values less than 20 kJ mol^{-1}. This benefits it as a porous adsorbent for C_2H_2/C_2H_4 separation. Enhancing affinity by the incorporation of Na^+ can be reflected on the largely increased Q_{st} value from 7.68 kJ mol^{-1} for C_2H_2 upon **COF-ECUT-1** to 19.21 kJ mol^{-1} for C_2H_2 upon **Na@COF-ECUT-1** at zero coverage.[37]

To further estimate their C_2H_2/C_2H_4 separation potential, we performed the transient breakthrough simulations for a C_2H_2/C_2H_4 mixture (1/99, v/v) upon **COF-ECUT-1** and **Na@COF-ECUT-1** materials with a total pressure of 100 kPa and a temperature of 298 K.[38] For the breakthrough simulations, the following parameter values were used: length of the packed bed, L = 0.3 m, void age of the packed bed, ε = 0.4, and superficial gas velocity at the inlet, u = 0.04 m s^{-1}. The simulated result is shown in Fig. 6. For **COF-ECUT-1**, the C_2H_2/C_2H_4 binary mixture is effectively separated and shows a long interval with $\Delta\tau$ = 160, whereas **Na@COF-ECUT-1** enables a longer interval with $\Delta\tau$ = 496, suggesting a three-fold enhancement in the potential of C_2H_2/C_2H_4 separation (Fig. 6).

As discussed above, the adsorption and next separation performance of porous adsorbents with open metal sites can be largely affected by moisture. We thus carried out the C_2H_2 gas adsorption of the activated samples of **Na@COF-ECUT-1** after leaving it in air for 24 h. Even under these conditions the C_2H_2 adsorption isotherm is fully recovered (Fig. S11†), strongly suggesting the negligible effect of moisture on the C_2H_2 adsorption performance.

To further investigate the mechanism of why both **COF-ECUT-1** and **Na@COF-ECUT-1** enable good C_2H_2/C_2H_4 separation performance, we carried out DFT calculation. Table S1† shows the adsorption energy and binding energy for **COF-ECUT-1** and **Na@COF-ECUT-1** with loading C_2H_2 or C_2H_4 molecules. It is clear that the C_2H_2 adsorption was preferred over C_2H_4 adsorption in both of them, in line with the experiment results that both of them afford selective adsorption of C_2H_2 over C_2H_4. Moreover, the incorporation of Na^+ into the COF enhancing the binding energy with both C_2H_2 and C_2H_4 molecules was observed, agreeing with the experimental results that are relative to **COF-ECUT-1**, and the Na^+-anchored counterpart of **Na@COF-ECUT-1** shows 1.6-fold or 1.7-fold improvement in the C_2H_2 or C_2H_4 adsorption capacity, respectively. For **Na@COF-ECUT-1**, the loading C_2H_2 molecule gives a higher binding energy than the C_2H_4 molecule, strongly supporting the experimental results of enhanced C_2H_2/C_2H_4 selectivity up to 9.41.

In the C_2H_2- and C_2H_4-loaded optimal structures (Fig. 7), the structural evidence for the selective adsorption of C_2H_2 over C_2H_4 was also revealed. For **COF-ECUT-1**, both C_2H_2 and C_2H_4 molecules are adsorbed around the SO_3H group with a hydrogen bond. The C_2H_2 molecule as a H-donor affords two strong hydrogen bonds with two SO_3H oxygen groups with a C···O distance of 2.798 (6) Å (Fig. 7a), whereas the C_2H_4 molecule as both the H-donor and H-acceptor just affords three weak hydrogen bonds with two SO_3H oxygen or OH units with a C···O distance of 3.755 (6) Å or 3.340(6) Å (Fig. 7b). Thereby, preferential or selective C_2H_2 adsorption over C_2H_4 adsorption can be reasonably realized. On the other hand, for **Na@COF-ECUT-1**, the driving force for both C_2H_2 and C_2H_4 molecules on COFs turns out to be coordination interactions between Na^+ and loaded guest molecules *via* Na–π interactions.

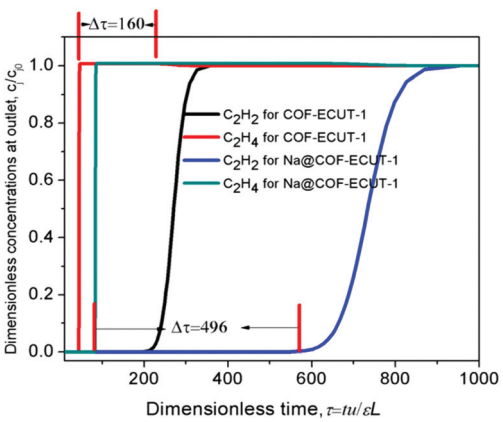

Fig. 6 Transient breakthrough simulations for the separation of the C_2H_2/CO_2 mixture (1/99, v/v) using materials **COF-ECUT-1** and **Na@COF-ECUT-1** at 298 K.

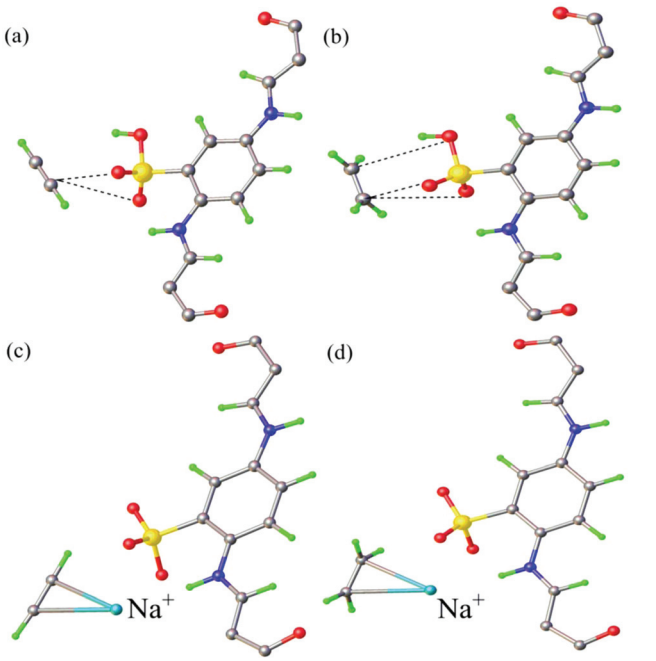

Fig. 7 View of the C_2H_2- and C_2H_4-loaded optimal structures in **COF-ECUT-1** (a and b) and **Na@COF-ECUT-1** (c and d).

Thereby, large enhancement in both C_2H_2 and C_2H_4 adsorption capacities was observed in the experimental results. Viewed from the bond length of Na–π interactions (2.777 (8) Å and 2.937 (8) Å for C_2H_2 (Fig. 7c); 2.829 (8) Å and 2.959 (8) Å for C_2H_4 (Fig. 7d)), it is obvious that stronger Na–π interactions is observed for C_2H_2 over C_2H_4, finally leading to a largely enhanced C_2H_2/C_2H_4 selectivity up to 9.41.

Conclusions

In conclusion, we demonstrate in this work a simple and general method by means of doping low-content Na^+ ions into COFs to enhance C_2H_2/C_2H_4 separation potential. The results show that the incorporation of Na^+ into the COF can significantly enhance C_2H_2 uptake capacity but with almost no decrease in selectivity; these advantages are further confirmed by transient breakthrough simulations. The use of DFT calculations affords deeper insights into the relationship between adsorption/separation performance and special structures such as SO_3H units in **COF-ECUT-1** and Na^+ in **Na@COF-ECUT-1**. This work outlines a promising approach for the use of COFs as adsorbents, enabling us to design and prepare COFs with excellent gas storage and separation performance.

Conflicts of interest

There are no conflicts to declare.

Acknowledgements

We thank the National Science Foundations of China (21871047 and 21661001) and the Natural Science Foundation of Jiangxi Province of China (20181ACB20003).

Notes and references

1 H. Li, L. B. Li, R. B. Lin, W. Zhou, S. C. Xiang, B. L. Chen and Z. J. Zhang, *Energy Chem.*, DOI: 10.1016/j.enchem.2019.100006.
2 H.-M. Wen, B. Li, H. Wang, C. Wu, K. Alfooty, R. Krishna and B. Chen, *Chem. Commun.*, 2015, **51**, 5610–5613.
3 D. Lv, R. Shi, Y. Chen, Y. Wu, H. Wu, H. Xi, Q. Xia and Z. Li, *ACS Appl. Mater. Interfaces*, 2018, **10**, 8366–8373.
4 H. Molero, B. F. Bartlett and W. T. Tysoe, *J. Catal.*, 1999, **181**, 49–56.
5 Y. He, R. Krishna and B. Chen, *Energy Environ. Sci.*, 2012, **5**, 9107–9120.
6 S. Yang, A. J. Ramirez-Cuesta, R. Newby, V. Garcia-Sakai, P. Manuel, S. K. Callear, S. I. Campbell, C. C. Tang and M. Schröder, *Nat. Chem.*, 2014, **7**, 121–129.
7 R. Zhang, B. Zhao, L. Ling, A. Wang, C. K. Russell, B. Wang and M. Fan, *ChemCatChem*, 2018, **10**, 2424–2432.
8 W. K. Lewis, E. R. Gilliland, B. Chertow and W. Milliken, *J. Am. Chem. Soc.*, 1950, **72**, 1157–1159.
9 A. Kodde, J. J. Padin, P. J. van der Meer, M. C. Mittelmeijer-Hazeleger, A. Bliek and R. T. Yang, *Ind. Eng. Chem. Res.*, 2000, **39**, 3108–3111.
10 S. Yuan, L. Feng, K. Wang, J. Pang, M. Bosch, C. Lollar, Y. Sun, J. Qin, X. Yang and P. Zhang, *Adv. Mater.*, 2018, **30**, 1704303.
11 B. Li, H.-M. Wen, W. Zhou, J. Q. Xu and B. Chen, *Chem*, 2016, **1**, 557–580.
12 Y. Cui, B. Li, H. He, W. Zhou, B. Chen and G. Qian, *Acc. Chem. Res.*, 2016, **49**, 483–493.
13 Z. Bao, G. Chang, H. Xing, R. Krishna, Q. Ren and B. Chen, *Energy Environ. Sci.*, 2016, **9**, 3612–3641.
14 (*a*) H. Q. Wu, C. S. Yan, F. Luo and R. Krishna, *Inorg. Chem.*, 2018, **57**, 3679–3682; (*b*) W. H. Yin, Y. Y. Xiong, H. Q. Wu, Y. Tao, L. X. Yang, J. Q. Li, X. L. Tong and F. Luo, *Inorg. Chem.*, 2018, **57**, 8722–8725; (*c*) M. B. Luo, Y. Y. Xiong, H. Q. Wu, X. F. Feng, J. Q. Li and F. Luo, *Angew. Chem., Int. Ed.*, 2017, **56**, 16376–16379; (*d*) F. Luo, C. Yan, L. Dang, R. Krishna, W. Zhou, H. Wu, X. Dong, Y. Han and T.-L. Hu, *J. Am. Chem. Soc.*, 2016, **138**, 5678–5684.
15 (*a*) Y.-J. Li, Y.-L. Wang and Q.-Y. Liu, *Inorg. Chem.*, 2017, **56**, 2159–2164; (*b*) H.-F. Ma, Q.-Y. Liu, Y.-L. Wang and S.-G. Yin, *Inorg. Chem.*, 2017, **56**, 2919–2925; (*c*) X.-K. Wang, J. Liu, L. Zhang, L.-Z. Dong, S.-L. Li, Y.-H. Kan, D.-S. Li and Y.-Q. Lan, *ACS Catal.*, 2019, **9**, 1726–1732; (*d*) J. Zhao, Y.-N. Wang, W.-W. Dong, Y.-P. Wu, D.-S. Li and Q.-C. Zhang, *Inorg. Chem.*, 2016, **55**, 3265–3271.
16 P.-Q. Liao, W.-X. Zhang, J.-P. Zhang and X.-M. Chen, *Nat. Commun.*, 2015, **6**, 8697–8705.
17 W. G. Cui, T. L. Hu and X. H. Bu, *Adv. Mater.*, 2019, 1806445.
18 Y. Zhang, L. Yang, L. Wang, S. Duttwyler and H. Xing, *Angew. Chem., Int. Ed.*, 2019, **58**, 8145–8150.
19 (*a*) Q.-G. Zhai, X. Bu, X. Zhao, D.-S. Li and P. Feng, *Acc. Chem. Res.*, 2017, **50**, 407–417; (*b*) Q.-G. Zhai, X. Bu, C. Mao, X. Zhao, L. Daemen, Y. Cheng, A. J. Ramirez-Cuesta and P. Feng, *Nat. Commun.*, 2016, **7**, 13645–13653; (*c*) X. Zhao, X. Bu, E. T. Nguyen, Q.-G. Zhai, C. Mao and P. Feng, *J. Am. Chem. Soc.*, 2016, **138**, 15102–15105.
20 H. Wang, X. Dong, V. Colombo, Q. Wang, Y. Liu, W. Liu, X. L. Wang and X. Y. Huang, *Adv. Mater.*, 2018, **30**, 1805088.
21 S.-C. Xiang, Z. J. Zhang, C.-G. Zhao, K. L. Hong, X. B. Zhao, D.-R. Ding, M.-H. Xie, C.-D. Wu, M. C. Das, R. Gill, K. M. Thomas and B. L. Chen, *Nat. Commun.*, 2011, **2**, 204–210.
22 B. Li, X. L. Cui, D. O'Nolan, H.-M. Wen, M. D. Jiang, R. Krishna, H. Wu, R. B. Lin, Y. S. Chen, D. Q. Yuan, H. B. Xing, W. Zhou, Q. L. Ren, G. D. Qian, M. J. Zaworotko and B. L. Chen, *Adv. Mater.*, 2017, **29**, 1704210.
23 X. Cui, K. Chen, H. Xing, Q. Yang, R. Krishna, Z. Bao, H. Wu, W. Zhou, X. Dong and Y. Han, *Science*, 2016, **353**, 141–144.

24 (*a*) C. B. Fan, L. Le Gong, L. Huang, F. Luo, R. Krishna, X. F. Yi, A. M. Zheng, L. Zhang, S. Z. Pu, X. F. Feng, M. B. Luo and G. C. Guo, *Angew. Chem., Int. Ed.*, 2017, **56**, 7900–7906; (*b*) C. B. Fan, Z. Q. Liu, L. Le Gong, A. M. Zheng, L. Zhang, C. S. Yan, H. Q. Wu, X. F. Feng and F. Luo, *Chem. Commun.*, 2017, **53**, 763–766.

25 S.-Y. Ding and W. Wang, *Chem. Soc. Rev.*, 2013, **42**, 548–568.

26 Y. Song, Q. Sun, B. Aguila and S. Ma, *Adv. Sci.*, 2019, **6**, 1801410.

27 Y. Yuan and G. Zhu, *ACS Cent. Sci.*, 2019, **5**, 409–418.

28 X. Guan, H. Li, Y. Ma, M. Xue, Q. Fang, Y. Yan, V. Valtchev and S. Qiu, *Nat. Chem.*, 2019, **11**, 587–594.

29 K. Chen and C. D. Wu, *Angew. Chem., Int. Ed.*, 2019, **58**, 8119–8123.

30 E. Jin, Z. Lan, Q. Jiang, K. Geng, G. Li, X. Wang and D. Jiang, *Chem*, 2019, **5**, 1632–1647.

31 (*a*) Q. Sun, B. Aguila, L. D. Earl, C. W. Abney, L. Wojtas, P. K. Thallapally and S. Ma, *Adv. Mater.*, 2018, **30**, 1705479; (*b*) Y. Yuan, Y. Yang, X. Ma, Q. Meng, L. Wang, S. Zhao and G. Zhu, *Adv. Mater.*, 2018, **30**, 1706507; (*c*) B. Aguila, Q. Sun, J. A. Perman, L. D. Earl, C. W. Abney, R. Elzein, R. Schlaf and S. Ma, *Adv. Mater.*, 2017, **29**, 1700665; (*d*) X. H. Xiong, Z. W. Yu, L. L. Gong, Y. Tao, Z. Gao, L. Wang, W. H. Yin, L. X. Yang and F. Luo, *Adv. Sci.*, 2019, **6**, 1900547; (*e*) Q. Pan, J. X. Li, F. T. Chi, Y. Xie, S. J. Yu, C. L. Xiao, F. Luo, J. Wang, X. L. Wang, C. L. Chen, W. S. Wu, W. Q. Shi, S. A. Wang and X. K. Wang, *Sci. China: Chem.*, 2019, **62**, 933–967.

32 C. J. Doonan, D. J. Tranchemontagne, T. G. Glover, J. R. Hunt and O. M. Yaghi, *Nat. Chem.*, 2010, **2**, 235–238.

33 X. Han, J. Huang, C. Yuan, Y. Liu and Y. Cui, *J. Am. Chem. Soc.*, 2018, **140**, 892–895.

34 L. Jiang, Y. Tian, T. Sun, Y. Zhu, H. Ren, X. Zou, Y. Ma, K. R. Meihaus, J. R. Long and G. Zhu, *J. Am. Chem. Soc.*, 2018, **140**, 15724–15730.

35 Y. Lu, J. He, Y. Chen, H. Wang, Y. Zhao, Y. Han and Y. Ding, *Macromol. Rapid Commun.*, 2018, **39**, 1700468.

36 J. Li, L. Jiang, S. Chen, A. Kirchon, B. Li, Y.-S. Li and H.-C. Zhou, *J. Am. Chem. Soc.*, 2019, **141**, 3807–3811.

37 (*a*) H. Cui, S. M. Chen, H. Arman, Y. X. Ye, A. Alsalme, R. B. Lin and B. L. Chen, *Inorg. Chim. Acta*, 2019, **495**, 118938 (1–5); (*b*) Y. X. Ye, H. Zhang, L. J. Chen, S. M. Chen, Q. J. Lin, F. F. Wei, Z. J. Zhang and S. C. Xiang, *Inorg. Chem.*, 2019, **58**, 7754–7759.

38 (*a*) R. Krishna, *Microporous Mesoporous Mater.*, 2014, **185**, 30–50; (*b*) R. Krishna, *RSC Adv.*, 2015, **5**, 52269–52295; (*c*) R. Krishna, *Sep. Purif. Technol.*, 2018, **194**, 281–300.

Electronic Supplementary Material (ESI) for Inorganic Chemistry Frontiers.

Enhancing C_2H_2/C_2H_4 separation by incorporating low-content sodium in covalent organic framework

Yuan Tao,[a] Rajamani Krishna,[b] Le Le Gong,[a] Li Xiao Yang,[a] Ya Ling Fan,[a] Li Wang,[a] Zhi Gao,[a] Jian Bo Xiong,[a] Li Jun Sun,[a] and Feng Luo[a]*

[a]State Key Laboratory for Nuclear Resources and Environment, and School of Biology, Chemistry and Material Science, East China University of Technology, Nanchang, Jiangxi 344000, China

[b]Van't Hoff Institute for Molecular Sciences, University of Amsterdam, Science Park 904, 1098 XH Amsterdam, The Netherlands

Table of Contents

S1. Materials and Instrumentation.

1,2-dichlorobenzene (99%), n-butanol (99%), phloroglucinol (99%), p-phenylenediamine (99%) and trifluoroacetic acid (99%) were purchased from Macklin (Shanghai) Inc. Hexamethylenetetramine (99%) was purchased from Alfa Aesar (Beijing) Co., Ltd. All other reagents were obtained from commercial suppliers and used as received unless otherwise noted.

Power X-ray diffraction（PXRD）patterns of samples were obtained at room temperature by a Bruker D8 ADVANCE X-ray at 40 mA and 40 kV using Cu Kα (λ = 1.5405 Å) radiations form 2° to 30° (2θ angle range), the simulated powder patterns were calculated by Mercury 1.4. The N_2 adsorption-desorption isotherms were obtained at 77 K on a Belsorp-max adsorption apparatus using ultrahigh-purity-grade (>99.999%) N_2. Each sample was degassed at 110 °C for 12 h under ultrahigh vacuum before measurement. Infrared spectra (IR) were performed in Thermo Scientific Nicolet iS5 FT-IR spectrometer with the 500-4000 cm^{-1}. Scanning electron microscope (SEM) and Energy Dispersive Spectrometer (EDS) was carried out on a Hitachi S-4800 microscope. Thermal gravimetric analysis (TGA) was performed by SDT Q600 TGA instrument from 30 to 800 °C in N_2 atmosphere at a constant rate of 10 °C/min. ^{13}C NMR spectra were recorded on Bruker Avance 600 MHz spectrometer. The C_2H_2 and C_2H_4 single-component adsorption isotherms with 99.999% purity gas were carried out at 298 and 273 K water bath on a Belsorp-max adsorption apparatus after degassed at 110 °C for 12 h under ultrahigh vacuum. Elemental analysis used PerkinElmer 2400 Series II CHNS under ultrahigh-purity-grade (>99.999%) He at 975 °C.

S2. Detailed experiment

Synthesis of 2,4,6-triformylphloroglucinol: To hexamethylenetetramine (15.098 g, 108 mmol) and phloroglucinol (6.014 g, 49 mmol) under N_2 was added 90 mL trifluoroacetic acid. The solution was heated at 100 ℃ for ca. 2.5 h. Approximately 150 mL of 3 M HCl was added and the solution was heated at 100 ℃ for 1 h. After cooling to room temperature, the solution was filtered through Celite, extracted with ca. 350 mL dichloromethane, dried over magnesium sulfate, and filtered. Rotary evaporation of the solution afforded 1.23 g (5.87 mmol ,11%) of an off-white powder. ^1H NMR indicated near 99% purity; a pure sample was obtained by sublimation. ^1H NMR (400 MHz, $CDCl_3$, 25 ℃) δ14.12 (s, 1H, OH), 10.15 (s, 1H, CHO) ppm. ^{13}C NMR (100 MHz, $CDCl_3$, 25 ℃) δ 192.01 (CHO), 173.57 (Ph-C2), 102.91 (Ph-C1) ppm. Calcd for C,51.44; H, 2.88; N, 0.00. Found: C 51.38; H 2.80; N, 0.00.

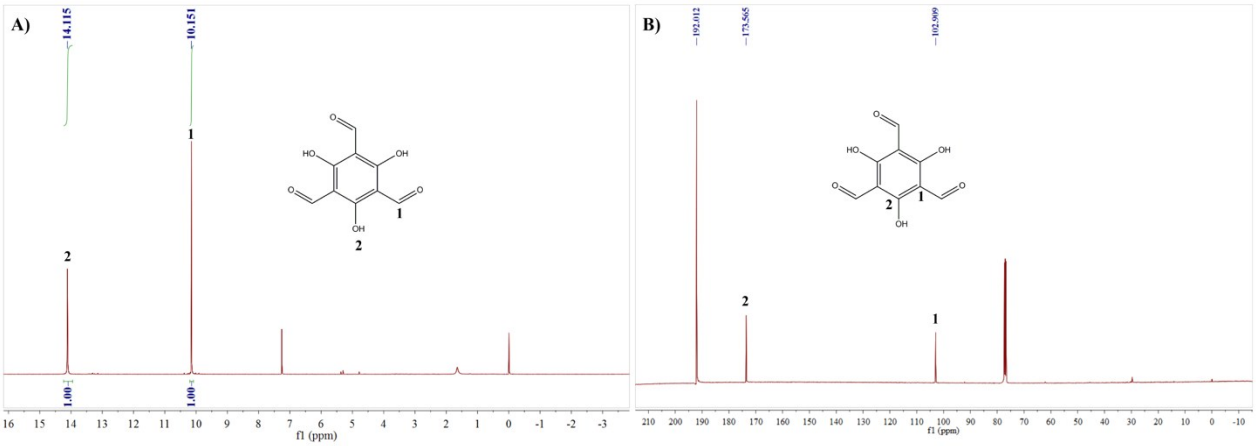

Fig. S1 A) ^{1}H NMR (400 MHz, $CDCl_3$, 25 ℃) spectrum of 2,4,6-triformylphloroglucinol. B) ^{13}C NMR (100 MHz, $CDCl_3$, 25 ℃) spectrum of 2,4,6-triformylphloroglucinol.

Synthesis of 2,5-diaminobenzenesulfonic acid: To p-phenylenediamine (2.7 g, 25 mmol) was add 20% fuming sulfuric acid (33 g, 66 mmol). The solution was heated at 145 ℃ for ca. 7 h. Approximately 4 mL deionized water was added, and the solution was heated at 135 ℃ for 3 h. Cooling to 30 ℃ for static crystallization for 2 h. Approximately 2 mL deionized water was added and adjusted pH 4 to 5 with 30% sodium hydroxide. Cooled to 10 ℃ and filtered to obtain a product 3.8 g（20 mmol，80%）, HPLC purity is greater than 98%. ^{1}H NMR (400 MHz, DMSO, 25 ℃) δ 7.38 (d, 1H, Ph-H1), 6.92 (dd, 1H, Ph-H3), 6.79 (d, 1H, Ph-H2), 4.55-9.10 (br., 4H, NH_2) ppm. ^{13}C NMR (100 MHz, DMSO, 25 ℃) δ 139.50 (Ph-C4), 131.15 (Ph-C2), 123.41 (Ph-C1), 122.04 (Ph-C5), 120.56 (Ph-C6), 117.78 (Ph-C3) ppm. Calcd for C, 38.29; H, 4.28; N, 14.88; S, 17.04. Found: C 38.26; H 4.29; N, 14.83; S, 17.02.

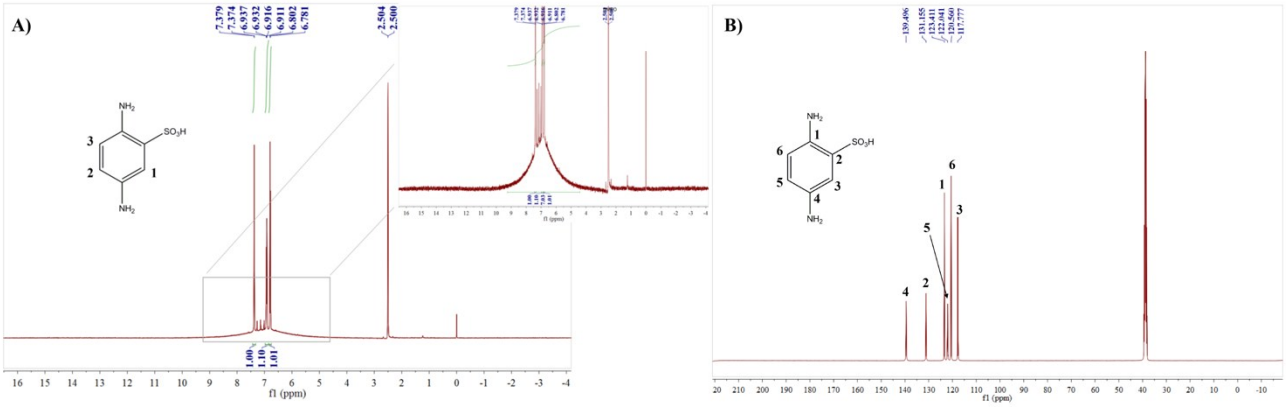

Fig. S2 A) ^{1}H NMR (400 MHz, DMSO, 25 ℃) spectrum of 2,5-diaminobenzenesulfonic acid. B) ^{13}C NMR (100 MHz, DMSO, 25 ℃) spectrum of 2,5-diaminobenzenesulfonic acid.

Synthesis of COF-ECUT-1. A mixture of 2,4,6-triformylphloroglucinol (63 mg, 0.3 mmol) and 2,5-diaminobenzenesulfonic acid (84.7 mg, 0.45 mmol) and a drop of n-butanol: 1,2-dichlorobenzene (1:1 v/v) was taken in Pyrex tube. The mixture was sonicated for 20 min, followed by addition of 0.5 mL of 3 M aqueous acetic acid. After that, the tube was degassed by freeze−pump−thaw cycles for three times, sealed under vacuum and heated at 120 °C for 3 days. The reaction mixture was cooled

to room temperature and washed with deionized water, dimethylacetamide and acetone. The resulting dark red powder was dried at 60 °C under vacuum for 12 hours.

Synthesis of Na@COF-ECUT-1. 100 mg COF-SO_3H added in 20 mL glass bottles with 1 M sodium carbonate solution for 30 hours. Then the resulted solid samples were washed with deionized water and methanol, and further dried at 60 °C under vacuum for 12 hours.

DFT calculation method. The periodic density functional theory calculations were performed by using the Vienna Ab initio Simulation Package (VASP) code.[1] The Perdew-Burke-Ernzerhof (GGA-PBE) functional was utilized to calculate the exchange-correlation energy, and the project-augmented wave generalized gradient approximation (PAW-GGA) pseudopotentials were adopted to describe the electron-ion interaction.[2-3] All the structures were optimized aiming to the global energy minimum, fully relaxed until the residual force convergence value on each tom being less 0.05 eV/Å. The Brillouin zone was sampled by *3 x 3 x 1* Gamma k-point mesh and the wave functions were expanded using a plane-wave basis set with kinetic energy cutoff of 500 eV. Spin-polarization was calculations with the lowest energy magnetic configurations were identified. All of the above structures were established by Materials Studio.

The binding energy was calculated follow:

$$E_b = E_{*g} - E_* - E_g \times n$$

Where the E_b means binding energy, E_{*g} represents the ground state energy after loading gas molecules, the E_* is the energy of cleanly unabsorbed and the E_g is the energy of pure gas at standard conditions, n represents the number of the gas molecules are adsorbed in COF pores.[4]

Table S1. The binding energy (eV) of these COFs with loading of guest molecules.

	E_*	$E_{*C_2H_2}$	$E_{*C_2H_4}$	$E_{C_2H_2}$	$E_{C_2H_4}$	$E_b^{C_2H_2}$	$E_b^{C_2H_4}$
COF-SO_3H	-1144.16	-1282.34	-1336.33	-22.93	-31.96	-0.60	-0.41
COF-SO_3Na	-1144.45	-1284.42	-1338.30	-22.93	-31.96	-2.39	-2.09

S3. TGA curve

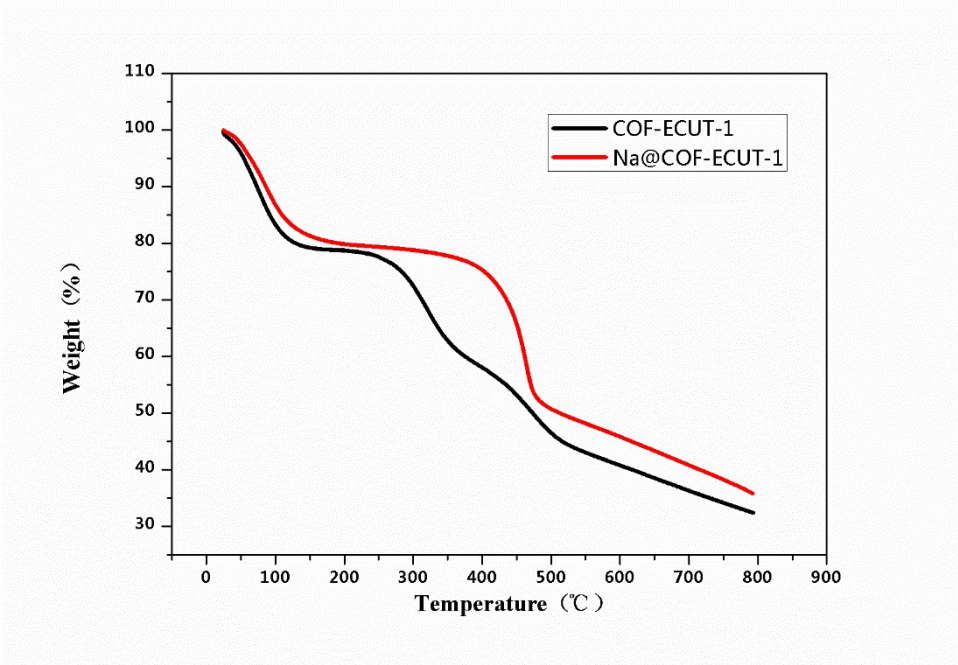

Fig. S3 TG data of **COF-ECUT-1** and **Na@COF-ECUT-1** under N_2 atmosphere.

S4. FT-IR spectrum of COFs

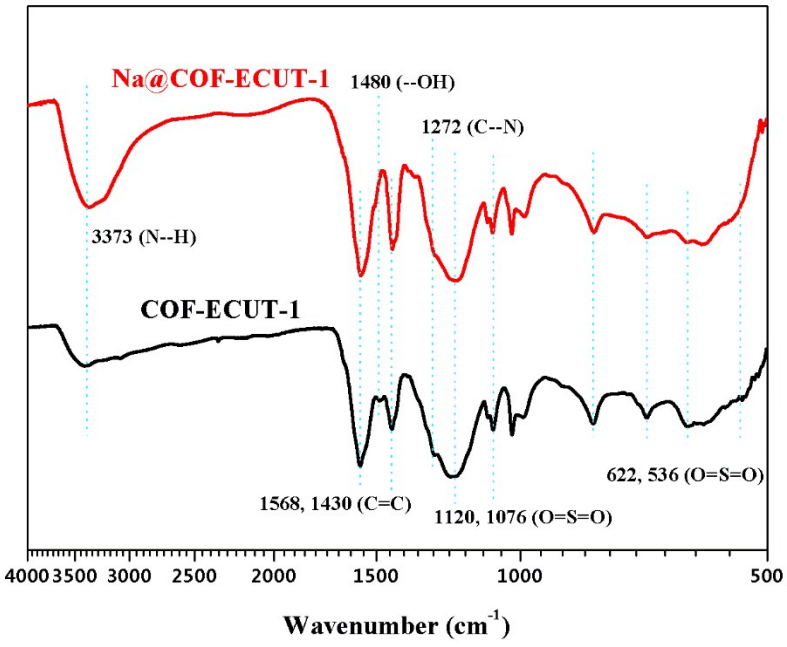

Fig. S4 IR spectrum of **COF-ECUT-1** and **Na@COF-ECUT-1**.

S5. Solid state ^{13}C NMR spectrum of COFs

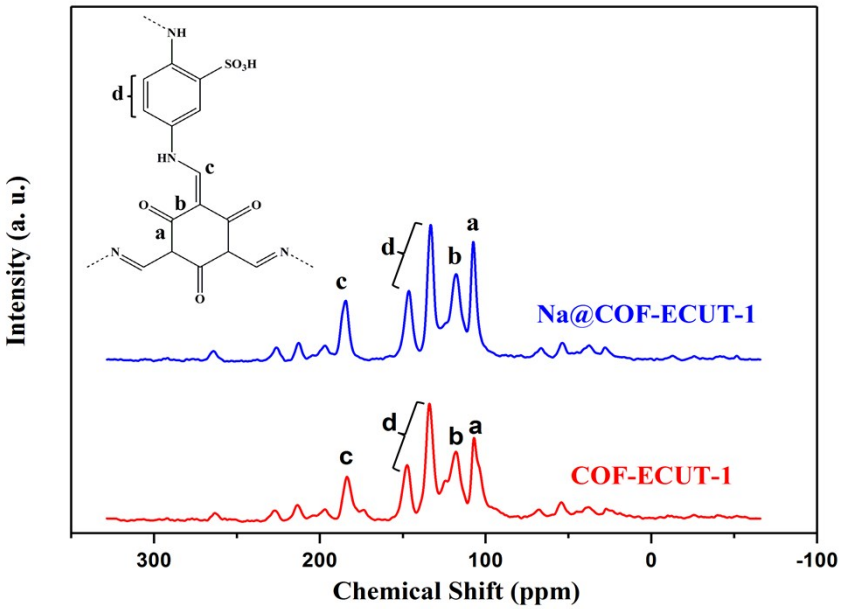

Fig. S5 ^{13}C CP/MAS NMR spectrum of **COF-ECUT-1** and **Na@COF-ECUT-1**.

S6. XRD analysis

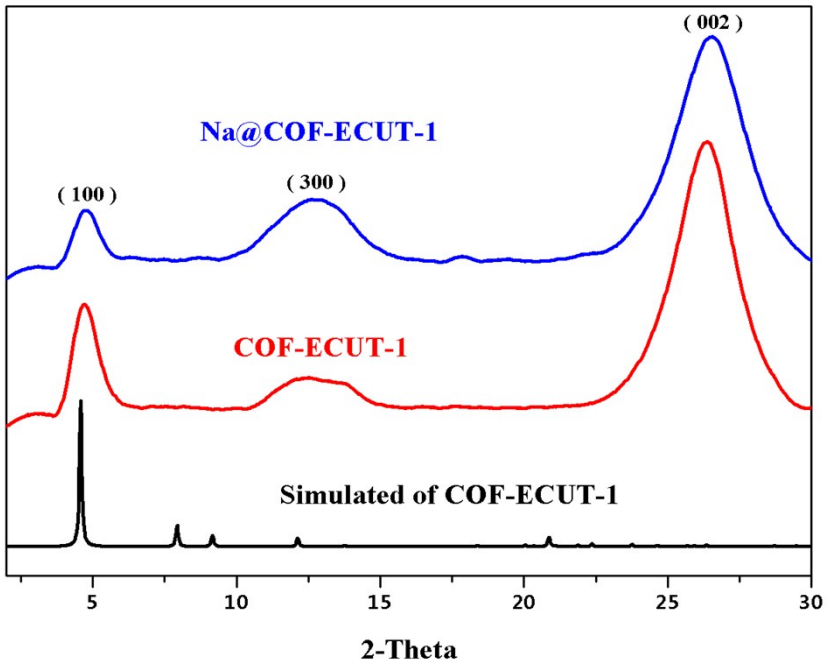

Fig. S6 The simulated and measured PXRD patterns of **COF-ECUT-1** and **Na@COF-ECUT-1**.

S7. View of the COF-ECUT-1 structure

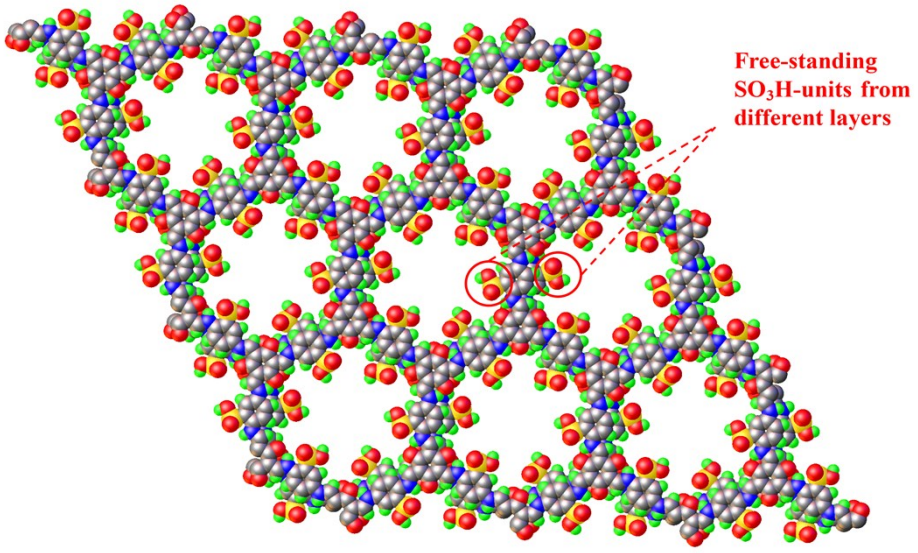

Fig. S7 View of the **COF-ECUT-1** structure with free-standing SO_3H-units from different layers.

S8. Gas adsorption studies of COFs

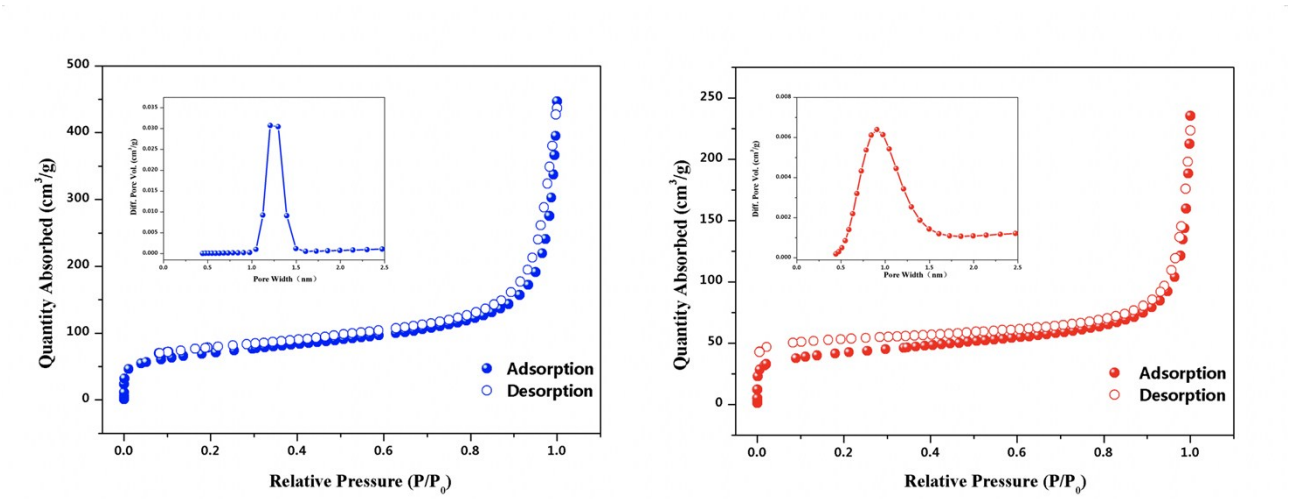

Fig. S8 Left: N_2 adsorption-desorption isotherms (77 K) of **COF-ECUT-1** with the inset of the distribution of pore size. Right: N_2 adsorption-desorption isotherms (77 K) of **Na@COF-ECUT-1** with the inset of the distribution of pore size.

S9. Isosteric heats of adsorption of COF-ECUT-1

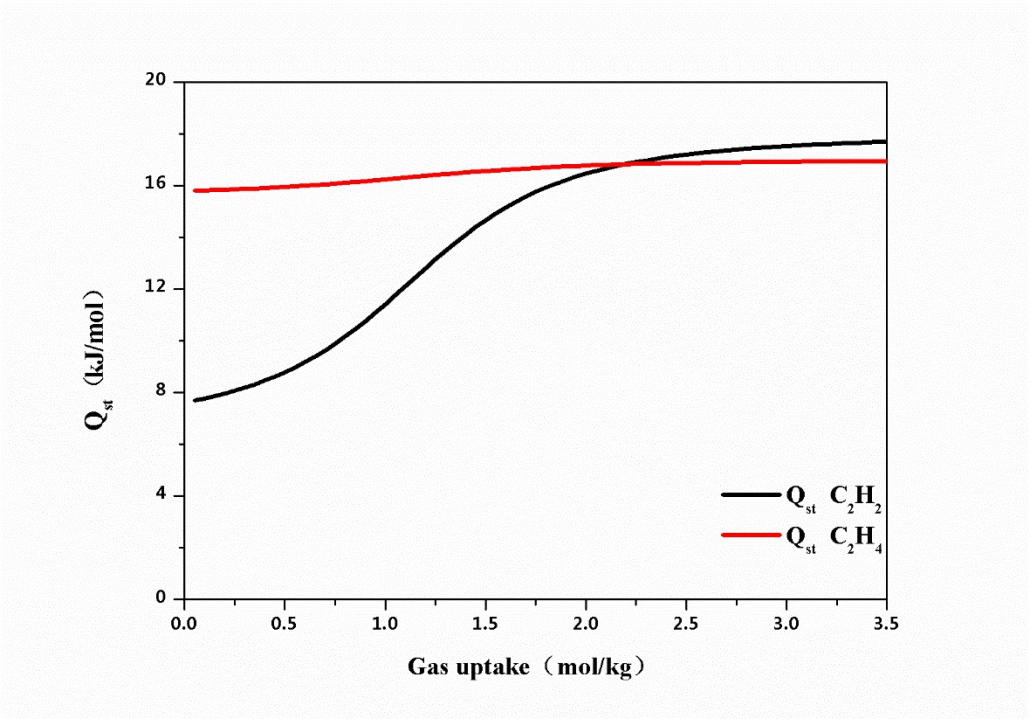

Fig. S9 Isosteric heats of adsorption for C_2H_2 (black) and C_2H_4 (red) of **COF-ECUT-1**.

S10. Isosteric heats of adsorption of Na@COF-ECUT-1

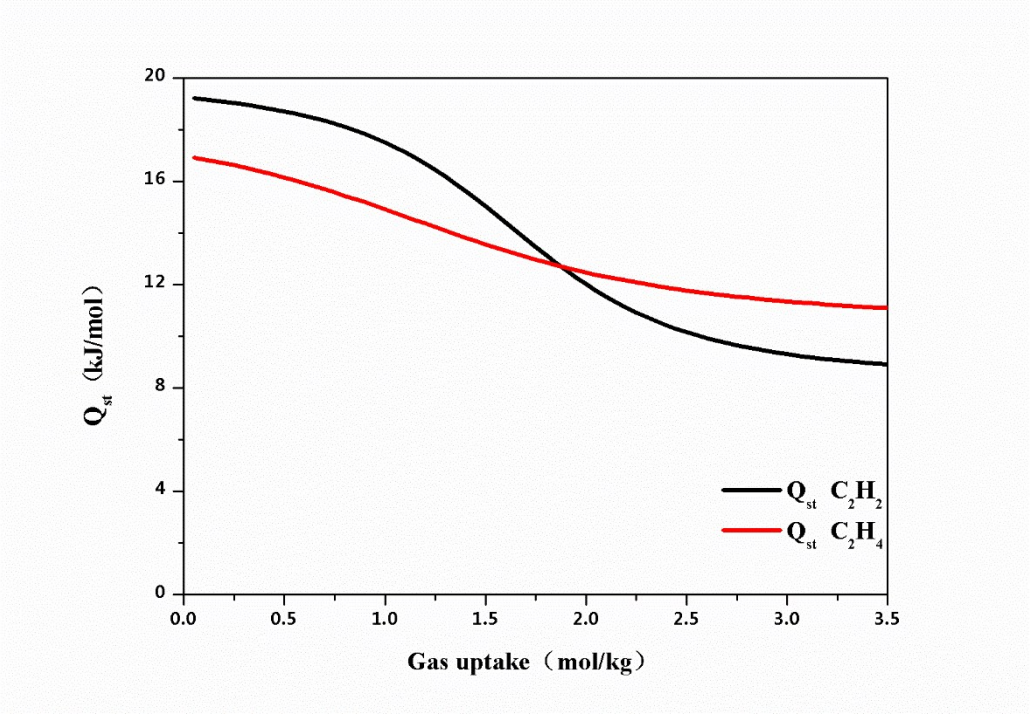

Fig. S10 Isosteric heats of adsorption for C_2H_2 (black) and C_2H_4 (red) of **Na@COF-ECUT-1**.

S11. Effect of moisture

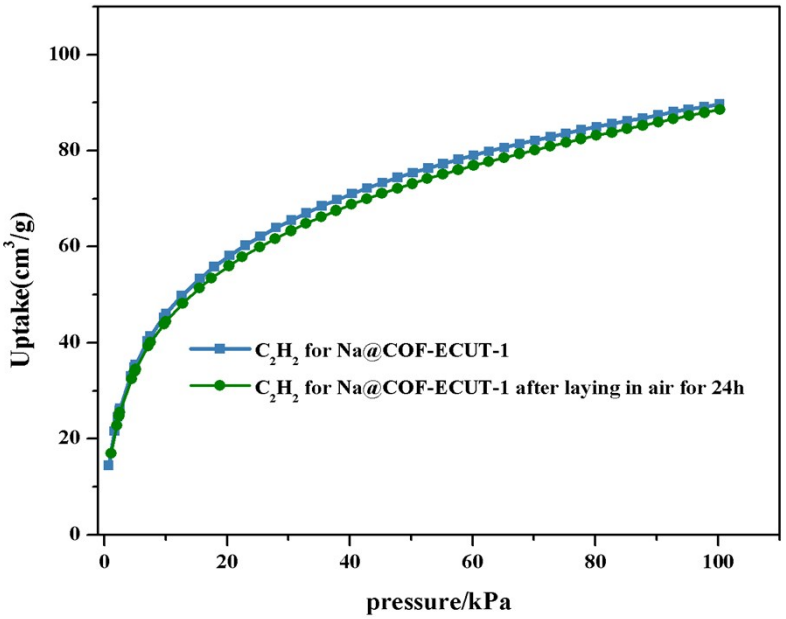

Fig. S11 A comparison of C_2H_2 adsorption for the samples of **Na@COF-ECUT-1** and the counterpart after laying in air for 24 h.

S12. References

1. G. Kresse and J. Hafner, *Phys. Rev. B*, 1993, **48**, 13115-13118.
2. S. Grimme, S. Ehrlich and L. Goerigk, *J. Comput. Chem.*, 2011, **32**, 1456-1465.
3. J. P. Perdew, K. Burke and M. Ernzerhof, *Phys. Rev. Lett.*, 1996, **77**, 3865-3868.
4. O. T. Qazvini, R. Babarao, Z. L. Shi, Y. B. Zhang and S. G. Telfer, *J. Am. Chem. Soc.*, 2019, **141**, 5014-5020.